CrystEngComm

ROYAL SOCIETY OF CHEMISTRY

PAPER

View Article Online
View Journal

Cite this: DOI: 10.1039/d5ce01193k

High-pressure neutron powder diffraction study of an arsenolite deuterium inclusion compound: structure and formation kinetics

Piotr A. Guńka, *[a] Maciej Dranka, [a] Christopher J. Ridley, [bc] Nicholas P. Funnell [b] and Craig L. Bull [bd]

Received 18th December 2025,
Accepted 6th March 2026

DOI: 10.1039/d5ce01193k

rsc.li/crystengcomm

High-pressure variable-temperature neutron powder diffraction was employed to investigate the synthesis and structural properties of arsenolite (As_4O_6), a cubic arsenic(III) oxide polymorph, and its inclusion compound with deuterium. The compound forms with the stoichiometry $As_4O_6{\cdot}2D_2$, consistent with earlier findings. At 295 K and 1.96(2) GPa, D_2 molecules occupy the 16*c* site (0, 0, 0) and are aligned along the <111> direction. The diffraction data suggest that the D_2 molecules at this site become rotationally disordered upon decompression to 0.78(2) GPa at 120 K, while no occupancy is observed at the 8*a* position ($\frac{1}{8}$, $\frac{1}{8}$, $\frac{1}{8}$) under any of the studied conditions. The kinetic data of the high-pressure inclusion compound synthesis at 1.56(2) and 1.96(2) GPa were analyzed using the Avrami model. The Avrami exponent, 0.135(16), remains invariant with pressure, demonstrating that the reaction topochemistry is unaffected by compression. Similarly, the reaction rates, 0.29(3) and 0.23(3) $min^{-0.135}$ at 1.56(2) and 1.96(2) GPa, respectively, exhibit negligible pressure dependence and suggest a surprisingly low activation volume of 1.6 $cm^3\ mol^{-1}$ for the reaction. These results provide detailed insight into the structural dynamics and kinetics of deuterium inclusion in arsenolite under high pressure.

Introduction

Current concerns about human impact on global warming have led to the quest for alternative energy sources to fossil fuels. A promising, well-studied alternative is hydrogen, which, when combined with oxygen, produces water. One of the key challenges in utilizing hydrogen as a power source is its storage, which has led to significant research efforts into materials that can store hydrogen efficiently and reversibly. It has recently been discovered that arsenolite, a molecular cubic polymorph of arsenic(III) oxide, forms inclusion compounds under high pressure (HP) both with hydrogen and helium ($As_4O_6{\cdot}2He$ and, most likely, $As_4O_6{\cdot}2H_2$, see Table S1 for their unit-cell parameters and volumes).[1–4] The gravimetric density of hydrogen within its inclusion compound with arsenolite is significantly lower than the U.S. Department of Energy's ultimate target (0.010 *vs.* 0.075 kg H_2 per kg system);[5] furthermore, the formation pressure of 1.5 GPa for the inclusion compound rules out its technological use. Nonetheless, it is a very good model system for basic research of hydrogen-storing materials due to its high crystallographic symmetry and relative simplicity.

The compound has been characterized to date using synchrotron X-ray diffraction, Raman spectroscopy, density functional theory (DFT) computations, and molecular dynamics (MD) simulations.[4,6] The crystal structure of the inclusion compound with hydrogen has been proposed based on its similarity to the inclusion compound with helium, whose structure could be determined using synchrotron X-ray diffraction.[4] Both compounds crystallize in the space group $Fd\bar{3}m$ with the stoichiometry $As_4O_6{\cdot}2X$, where *X* is He or H_2. The stoichiometry has been experimentally determined for helium and has been assumed for hydrogen. As shown in Fig. 1, the As_4O_6 molecule's center of mass occupies the special position 8*b*, exhibiting the symmetry of point group $\bar{4}3m$, and helium atoms or hydrogen molecules occupy the special position 16*c* of point group $\bar{3}m$.[1,4] There was no evidence from X-ray diffraction or DFT computations that hydrogen may occupy an additional site in the compound.[4] It follows from the Raman measurements of vibrons and molecular dynamics (MD) simulations that dihydrogen molecules are most likely aligned along the <111> direction. However, H_2 protons observed in the Raman spectra suggest that H_2 molecules rotate freely at room temperature, before settling along the <111> direction at low temperatures.[6]

[a] *Faculty of Chemistry, Warsaw University of Technology, Noakowskiego 3, Warszawa, 00-664, Poland. E-mail: piotr.gunka@pw.edu.pl*
[b] *ISIS Neutron and Muon Source, Rutherford Appleton Lab, Didcot, OX11 0QX, UK*
[c] *Neutron Scattering Division, Oak Ridge National Laboratory, Oak Ridge, Tennessee 37831, USA*
[d] *EastCHEM School of Chemistry, Joseph Black Building, David Brewster Road, Edinburgh, EH9 3FJ, UK*

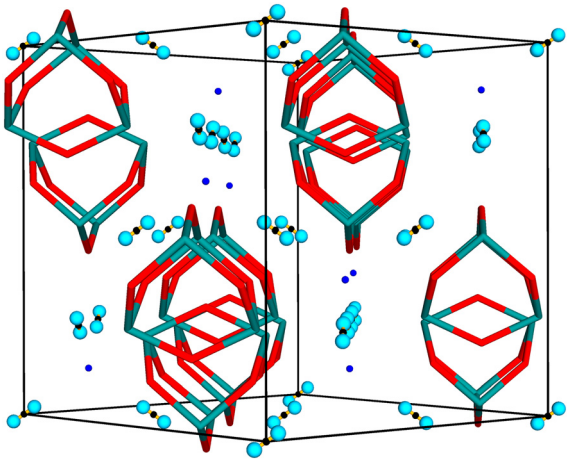

Fig. 1 Proposed crystal structure model of the arsenolite inclusion compound with hydrogen $As_4O_6{\cdot}2H_2$. As_4O_6 molecules represented in a wireframe model with As and O colored teal and red, respectively. H_2 molecules shown in a ball-and-stick model and aligned along the <111> direction. Small black and blue spheres denote 16*c* and 8*a* special positions, respectively, where H_2 molecules may be present in the structure.

Even though hydrogen most likely occupies only one crystallographic site in the crystal structure and no hopping between sites has been observed in MD simulations, there are three hydrogen vibrons in the recorded Raman spectra.[4,6] Two of the vibrons stem from the nuclear spin isomers *ortho* and *para*, while the origin of the third one remains unclear.[6]

The kinetics of the formation of arsenolite inclusion compounds have been extensively studied. Single-crystal X-ray diffraction revealed that the formation rate of the helium inclusion compound depends strongly on both the quality of the crystal used for the study and on the rate of pressure increase.[1,3] Two mechanisms of permeation were, therefore, proposed: slower penetration of helium into arsenolite *via* temporary channels formed by phonons and faster permeation of helium along the borders of mosaic blocks.[3] The growth rate of the inclusion compound $As_4O_6{\cdot}2H_2$ on a plate-like arsenolite single crystal was found to be linear, as determined by HP infrared spectroscopic measurements. Such behavior indicates that the reaction at the $As_4O_6/As_4O_6{\cdot}2H_2$ phase boundary, rather than diffusion, is the rate-limiting step.[7]

Herein, we report a high-pressure neutron powder diffraction study of the arsenolite inclusion compound with deuterium at variable temperatures. This study was conducted in a large-volume press, using a sample volume of *ca.* 30 mm^3, unlike in more popular diamond-anvil cell HP experiments, where volumes of less than 0.01 mm^3 are typically investigated. The stoichiometry and crystallographic symmetry of the compound were experimentally determined, and the hypothesis that deuterium may occupy multiple crystallographic sites was verified. The dynamics of D_2 molecules in the solid state were thoroughly investigated. The kinetics of inclusion compound formation for a powdered sample were also investigated and analyzed using the Avrami model.[8–10]

Results and discussion

Fig. 2 shows all of the neutron powder diffractograms (NPDs) obtained during the experiments in chronological order from top to bottom. The first pattern shows narrow reflections from arsenolite present in the PE press. The second pattern, recorded at 1.55(4) GPa, reveals the partial conversion of arsenolite into its deuterium inclusion compound. One may see that reflections of the inclusion compound appear at higher *d*-spacing and are broader, indicating reduced crystallinity or decreased crystallite size, resulting from the chemical reaction that took place. The reflections within the black rectangle spanning *d*-spacings between 3.1 and 3.4 Å are indicative of the presence of arsenolite or its inclusion in the sample (see Table S2 for the unit-cell parameters arsenolite and its inclusion compound). The difference in unit-cell volumes of arsenolite and its deuterium inclusion compound amounts to 138.6 $Å^3$ at 1.56(2) GPa and 153.2 $Å^3$ at 1.96(2) GPa. This is significantly more than that for the $As_4O_6{\cdot}2He$ inclusion compound with helium (100 $Å^3$ at 2 GPa)[3] and comparable to the inclusion compound with hydrogen (157 $Å^3$ at 1.5 GPa).[4] Rietveld refinements allowed for an unequivocal confirmation of the inclusion compound's space group symmetry $Fd\bar{3}m$. Some remnants of arsenolite can still be observed in the pattern recorded at 1.93(2) GPa at room temperature. Interestingly, when arsenolite was transformed to the inclusion compound, a broad feature appeared in the background where a strong {222} reflection from arsenolite had been present (d = 3.138 Å). Subsequently, the temperature was gradually lowered to 120 K, and the pressure was maintained at a relatively constant level. The patterns from the temperature ramp are noisier because they were collected for shorter times. Two long measurements were carried out at 120 K: at 1.68(3) GPa and after all the applied load on the PE press was removed. This yielded a pressure of 0.76(2) GPa inside the gas clamp as revealed by the determined lattice parameter of lead. The inclusion compound was still intact within the clamp 36 hours later under these p and T conditions. Then, the temperature was gradually increased, and the inclusion compound decomposed, reforming arsenolite between 150 and 200 K. Notably, arsenolite reflections are broader than initially seen, confirming a decrease in the crystallite size or a worsening of crystallinity during the process.

After initial Rietveld refinements, diffraction patterns of the arsenolite inclusion compound with various stoichiometries and various D_2 molecule orientations and dynamics have been simulated to investigate how these factors affect the patterns and whether it is possible to discriminate between them using our experimental data.

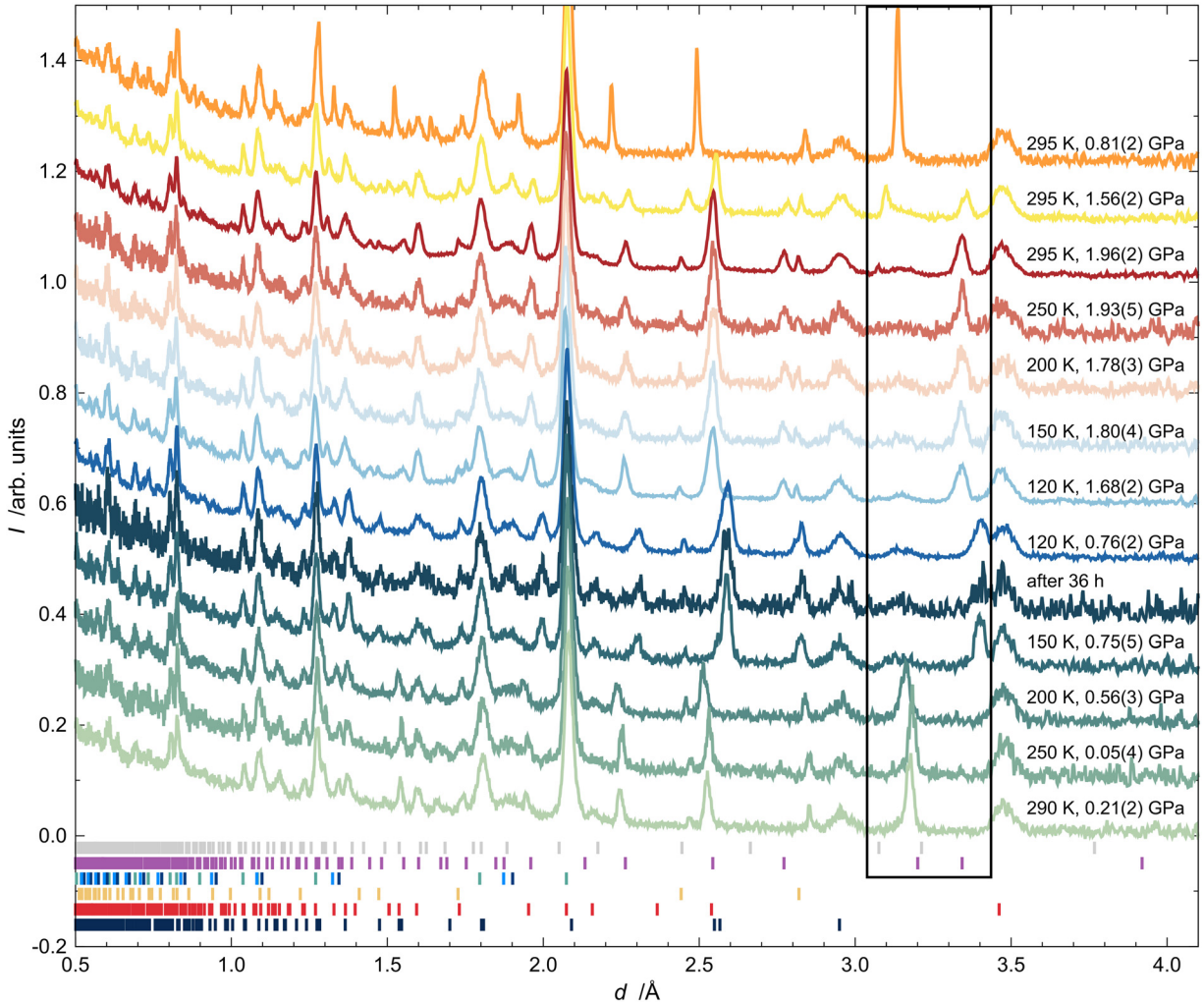

Fig. 2 TOF neutron powder diffraction patterns of arsenolite and its inclusion compound with deuterium. The pressure and temperature are given in labels on the right-hand side. The solid box shows the region with reflections indicative of the presence of arsenolite or its inclusion compound with deuterium. TOF can be obtained by multiplying the *d*-spacing by 4842.3 μs Å^{-1}. Ticks below the patterns denote the reflection positions of As_4O_6 (grey), $As_4O_6{\cdot}2D_2$ (violet), Cu, CuBe *bcc*1, CuBe *bcc*2 (all three in one line, green, light and dark blue, respectively), Pb (yellow), Al_2O_3 (red), and ZrO_2 (dark blue) at 295 K and 1.96(2) GPa. Note that there are small variations in the positions of reflections, particularly for arsenolite, its inclusion compound, and lead.

Neutron powder diffraction pattern simulation

The simulated TOF diffraction patterns of pure arsenolite and its inclusion compound with deuterium are presented in Fig. 3a. Only the *d*-spacing region from 2 to 4 Å is shown due to the significant overlap of inclusion compound reflections with the reflections coming from other phases present in the experimental setup at smaller *d*-spacings. Two different sites for D_2 molecules were considered: the 16*c* site, which is the most likely based on our earlier results and leads to the $As_4O_6{\cdot}2D_2$ stoichiometry, and the less probable 8*a* site, which leads to a smaller D_2 capacity $As_4O_6{\cdot}D_2$ (*cf.* Fig. 1). The differences between the simulated patterns for models with D_2 molecules at the 16*c* site, but with different orientations and dynamics, are plotted in Fig. 3b. It is evident that the orientation of D_2 molecules in the 16*c* site, denoted in the legend by crystallographic directions along which the D_2 dumbbell is aligned, exerts a negligible influence on the diffraction patterns (note the different *Y* scales in a and b). Only in the case of molecules aligned along the <111> direction (D atoms placed at *x*, *x*, *x*) are the molecules ordered. In the case of the <110> and <100> models (D atoms placed at *x*′, *x*′, 0 and *x*″, 0, 0, respectively), there is disorder into three components. The diffraction pattern from the <100> model resembles that from a model with a freely rotating D_2 molecule most. Notably, a model with a D_2 molecule at the 8*a* site yields a significantly different diffraction pattern with the {022} reflection showing substantial intensity, in stark contrast to pure arsenolite and the inclusion compound with D_2 molecules at the 16*c* site.

Subsequently, TOF diffraction patterns with D_2 molecules present at two sites were simulated. Rather unlikely models with fully occupied sites 16*c* and 8*a* are

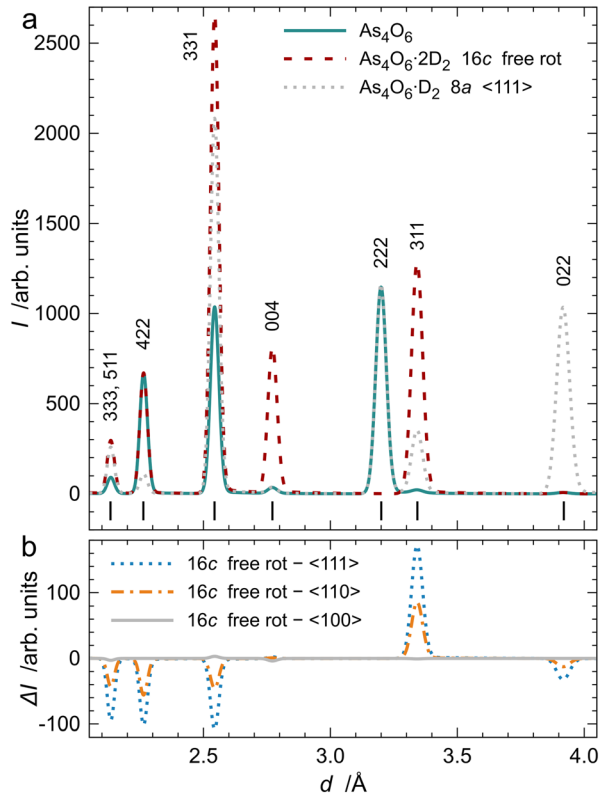

Fig. 3 Simulated TOF NPDs of arsenolite and its inclusion compound with deuterium placed at different sites (a). Differences between the simulated patterns for the $As_4O_6{\cdot}2D_2$ inclusion compound with freely rotating D_2 molecules in the 16*c* site and for structures with the molecules at the same site but aligned along different crystallographic directions indicated in the legend (b). Multiplicities and Wyckoff letters denote the sites of D_2 molecules, while <*uvw*> denotes the crystallographic directions along which the molecules are aligned. "Free rot" denotes a model with freely rotating D_2 molecules. The *hkl* indices of the reflections are listed next to each reflection. Ticks below the patterns indicate the positions of reflections for the simulated phases, which were all simulated with the same lattice parameter (*a*) to facilitate comparison.

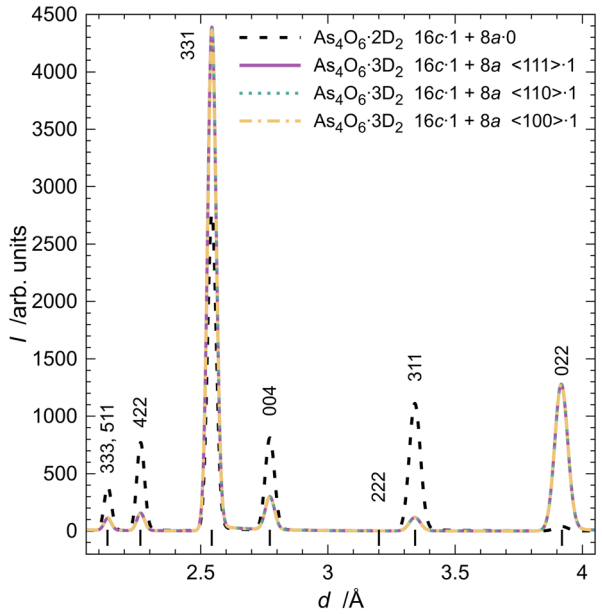

Fig. 4 Comparison of the simulated TOF NPDs for the inclusion compounds $As_4O_6{\cdot}2D_2$ and $As_4O_6{\cdot}3D_2$. The former contains D_2 molecules at the 16*c* site only, while the latter contains D_2 molecules at both sites, 16*c* and 8*a*. The coefficients denote occupancy of the particular site, whereas <*uvw*> denotes the crystallographic directions along which D_2 molecules are oriented at the 8*a* site. The D_2 molecules at the 16*c* site are aligned along the <111> direction. All phases were simulated with the same *a*-lattice parameter to facilitate comparison.

presented in Fig. 4. One can see that the orientation of D_2 molecules at the 8*a* site does not significantly affect the diffracted intensities, as is the case at the 16*c* site. It is noteworthy that, due to the presence of symmetry elements, D_2 molecules at the 8*a* site, exhibiting symmetry of point group $\bar{4}3m$, are disordered into four, six, and three components when molecules are aligned along the <111>, <110>, and <100> directions, respectively.

More likely structural models of the inclusion compound with the stoichiometry $As_4O_6{\cdot}2D_2$ and deuterium molecules distributed over the 16*c* and 8*a* sites were used for the last series of simulations, whose results are presented in Fig. 5. It is clear that the transfer of even small portions of D_2 molecules from the 16*c* to the 8*a* site leads to significant changes in the intensities of reflections that are diagnostic of the distribution of deuterium in the crystal structure.

Inclusion compound crystal structure studies at high pressure and variable temperature

The Rietveld fit of the initial pattern is presented in Fig. S2. NPDs recorded at 295 K and 1.93(2) GPa, as well as at 120 K and 0.76(2) GPa, together with Rietveld fits, are presented in Fig. 6 and 7.†,‡ Some traces of arsenolite remained at 1.96(2) GPa and 295 K, but they were completely transformed into the inclusion compound during cooling. As shown in the figures, the {022} reflection of the inclusion compound around 3.9 Å has zero intensity, indicating that no D_2 is present at the 8*a* site. Free refinement of D_2 occupancy at the 16c site yields one with small uncertainties at both 295 K and 120 K, confirming full occupation of the site and the stoichiometry $As_4O_6{\cdot}2D_2$. Initial refinements were carried out with restraints on D–D and As–O bond lengths,

† Crystal structure of $As_4O_6{\cdot}2D_2$ (M = 403.72 g mol^{-1}): cubic, space group $Fd\bar{3}m$ (no. 227, 2nd choice of origin), a = 11.0824(6) Å, V = 1361.1(2) Å^3, Z = 8, T = 295(1) K, p = 1.96(2) GPa. As (32*e*): x_{As} = 0.2686(4); O (48*f*): x_O = 0.2080(6); D (32*e*): x_D = 0.0207(7); $B_{isoAs/O}$ = 0.76(12) Å^2; B_{isoD} = 6.6(3); d_{As-O} = 1.798(5) Å; d_{D-D} = 0.80(3) Å.

‡ Crystal structure of $As_4O_6{\cdot}2D_2$ (M = 403.72 g mol^{-1}): cubic, space group $Fd\bar{3}m$ (no. 227, 2nd choice of origin), a = 11.2789(8) Å, V = 1434.8(3) Å^3, Z = 8, T = 120(1) K, p = 0.78(2) GPa. As (32*e*): x_{As} = 0.2772(5); O (48*f*): x_O = 0.2001(6); freely rotating D_2 (16*c*); $B_{isoAs/O/D_2}$ = 0.50 Å^2 (fixed); d_{As-O} = 1.786(5) Å; d_{D-D} = 0.7415 Å (fixed).

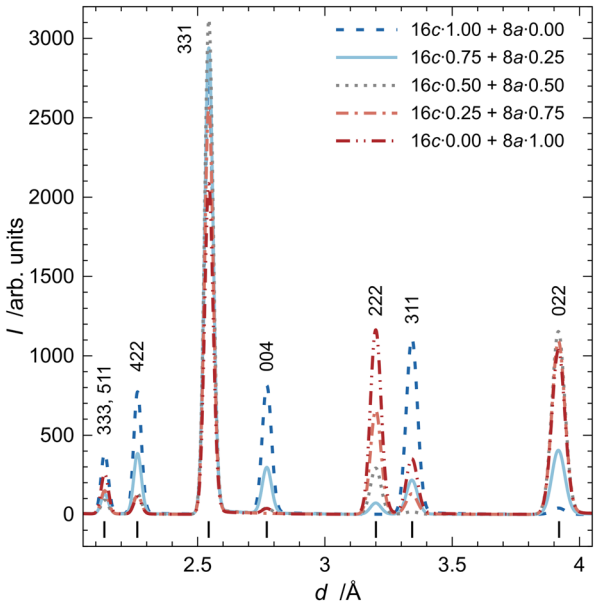

Fig. 5 Comparison of the simulated TOF NPDs for the inclusion compound $As_4O_6{\cdot}2D_2$ with deuterium molecules distributed with various proportions, denoted in the legend, between sites 16*c* and 8*a*. D_2 molecules are aligned along the <111> directions at both sites.

which were released in the final stages of the refinements. The final bond lengths at 295 K and 1.96(2) GPa are 0.80(3) and 1.798(5) Å for D–D and As–O bonds, respectively, which agree well with literature values.[1,11] The model with the D_2 molecule aligned along the <111> direction gave slightly better R_{wp} and GoF as well as better visual fit than the models with other orientations or free rotation of deuterium (see Table S3). It also agrees with previous molecular dynamics simulations.[6] In particular, the {311} reflection intensity is overestimated when D_2 is not aligned along <111>. However, at 120 K and 0.78(2) GPa, the experimental intensity of the {311} reflection was significantly higher than that predicted by this model, indicating a freely rotating D_2 molecule located at (0, 0, 0). Such a model indeed provides a better visual fit and is consistent with the expectation that pressure release should leave more space for D_2 molecules to rotate freely.

Determination of the rate of inclusion compound formation

The diffraction data at 1.56(2) and 1.96(2) GPa, shown in Fig. 2, were averaged from 10 and 25 separate runs, respectively, each lasting approximately 1 hour.§ For the kinetic investigation, the individual runs were reduced separately, resulting in 35 NPDs that showed the gradual formation of the inclusion compound. Rietveld refinements of the patterns, as described in the methodological section, yielded a conversion factor of arsenolite into the inclusion compound x, which is plotted as a function of time in Fig. 8.

There are three families of kinetic models for solid-state reactions: diffusion models, nuclei growth models, and phase boundary models.[12] The diffusion models were ruled out because our earlier study indicated that the reaction taking place at the phase boundary is the limiting step in the formation of the arsenolite inclusion compound with hydrogen.[7] The functions related to the conversion factor x and time t: $\ln(-\mathrm{d}(1-x)/\mathrm{d}t) = f(\ln(1-x))$ and $\ln(-\ln(1-x)) = f(t-t_0)$ are plotted in Fig. S3 and S4. Linear relationships were found for the latter function, indicating that nuclei growth models are mathematically appropriate for describing the data obtained.[12] Similarly as in other kinetic studies of HP reactions, the Avrami model from the nuclei growth model family has been applied: $x = 1 - e^{-b(t-t_0)^n}$.[13,14] The same values of n were obtained for both pressures, which indicates that the change in pressure does not affect the topochemistry of the reaction. Finally, fitting of all the data for both pressures was carried out with the following equations: $x = 1 - e^{-b_1(t-t_{01})^n}$ for the 1.56(2) GPa data and $x = 1 - e^{-b_2(t-t_{02})^n} + 1 - e^{-b_1(t_{02}-t_{01})^n}$ for the 1.96(2) GPa data. The second term in the latter equation reflects the presence of both unreacted arsenolite and the formed inclusion compound in the clamp when the pressure was increased to ~1.9 GPa. The final values of the fitted parameters are presented in Table 1.

The value of exponent n is significantly smaller than one, suggesting linear growth; however, no physical model resulting in n smaller than $\frac{1}{2}$ has been described,[15] even though values lower than $\frac{1}{2}$ have been observed experimentally in HP co-crystal polymerization, in recrystallization of alloys, and in MD simulations of intermetallic formation in supercooled conditions.[14,16,17] The $As_4O_6{\cdot}2D_2$ formation reaction begins abruptly upon pressure increase, but the rate decreases rapidly. It is possible that D_2 initially permeated worse-quality crystals or those whose quality deteriorated most due to HP-induced strains. There could also be pre-existing nuclei of the inclusion compound due to stochastic sorption of D_2 in arsenolite below 1.5 GPa, a process observed for urea in protium.[18] This hypothesis is supported by the fact that urea, similar to arsenolite, contains channels that are smaller than H_2 molecules, yet they are penetrated by these molecules at elevated pressure.[1,18] In other words, a certain number of nuclei were already present in the sample, and they grew very quickly. The formation of new nuclei at ~1.5 GPa was very slow, explaining the plateau around 0.5 in the $x = f(t)$ dependence. Then, upon increasing the pressure to ~1.9 GPa, a large number of new nuclei were formed, which also reacted quickly, leading to another plateau around 0.95. The rest of the

§ Note that the first six runs at 1.96(2) GPa (corresponding to the first six blue squares) were not averaged for the NPD pattern at 1.96(2) GPa used in the Rietveld refinement as the conversion was still changing significantly. Only the 19 remaining points were taken into account when variation in the conversion factor may be attributed to the experimental noise.

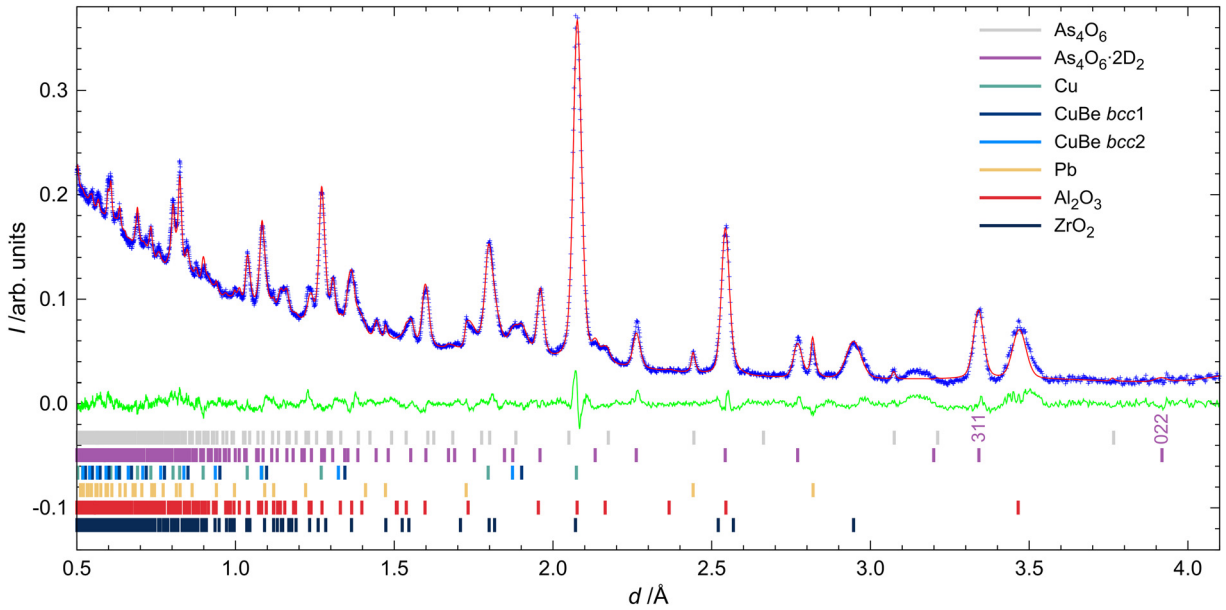

Fig. 6 TOF NPDs recorded at 295 K and 1.96(2) GPa. Blue crosses and red and green lines correspond to the experimental points, Rietveld fit curve, and the difference between the two, respectively. Ticks at the bottom denote the position of reflections of the phases listed in the legend. R_{wp} = 3.36%; GoF = 1.62.

arsenolite reacted upon cooling, which may have induced additional strains and/or defects in the crystals, *i.e.*, new nuclei, that facilitated the completion of the reaction.

The activation volume of the reaction can be calculated using the following relationship: $\Delta^{\ddagger}V = -RT\left(\frac{\partial(\ln b)}{\partial p}\right)_T$. The activation volume is estimated at 1.6 $cm^3\ mol^{-1}$ based on the reaction rates determined at 1.56(2) and 1.96(2) GPa, assuming linear dependence of $\ln b$ on pressure. This is surprisingly low, given that there are no permanent channels in the arsenolite crystal structure large enough for deuterium penetration and that it must be expanded to allow D_2 molecules, whose molar volume is ~10 $cm^3\ mol^{-1}$, to permeate between As_4O_6 molecules. It might also be that the assumption of a linear dependence of $\ln b$ on pressure is an oversimplification.

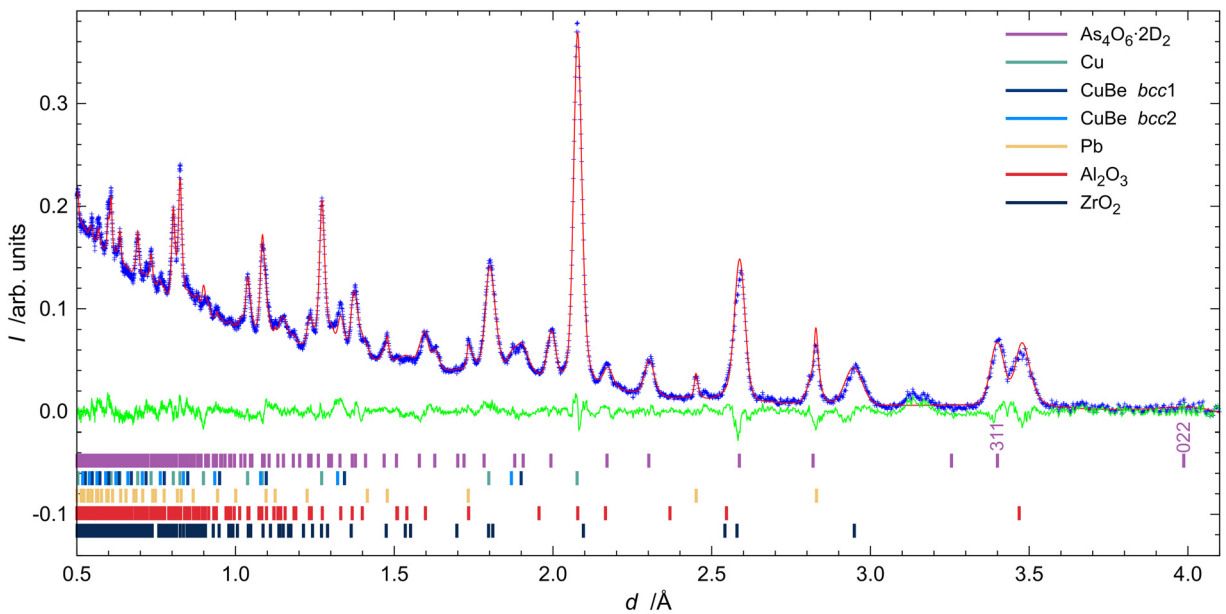

Fig. 7 TOF NPDs recorded at 120 K and 0.76(2) GPa. Blue crosses and red and green lines correspond to the experimental points, Rietveld fit curve, and the difference between the two, respectively. Ticks at the bottom denote the position of reflections of the phases listed in the legend. R_{wp} = 4.67%; GoF = 1.35.

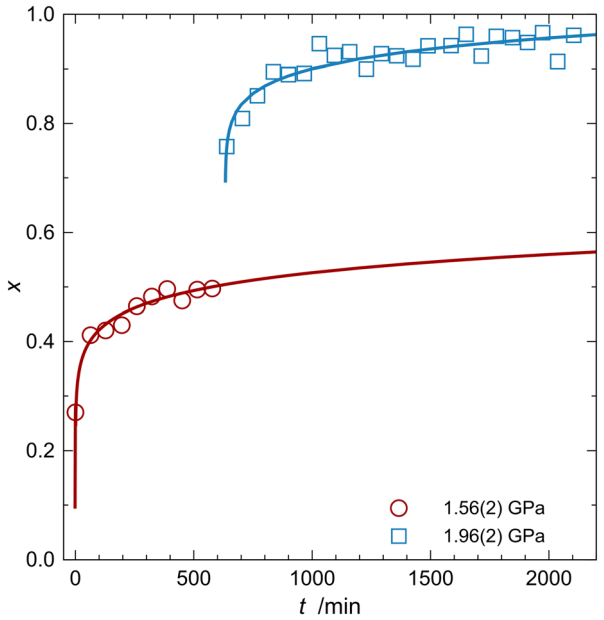

Fig. 8 Conversion factor x of arsenolite into the inclusion compound $As_4O_6{\cdot}2D_2$, plotted as a function of time for one sample measured subsequently at two pressures given in the legend. Circles and squares represent the experimental points, while solid lines represent the Avrami model fits (for details, see the main text).§

Table 1 The values of the fitted parameters of the Avrami model

p/GPa	1.56(2)	1.96(2)
b/min^{-n}	0.29(3)	0.23(3)
t_0/min	−1.7(14)	633(5)
n	0.135(16)	

Conclusions

High-pressure neutron powder diffraction measurements of arsenolite in deuterium were carried out. An inclusion compound with deuterium was formed *in situ* in a large-volume press used in this study, which not only enabled structural investigation of the compound but also quantitative analysis of reaction kinetics. The space group symmetry and stoichiometry of the formed inclusion compound were confirmed to be $Fd\bar{3}m$ and $As_4O_6{\cdot}2D_2$, respectively. D_2 molecules in the inclusion compound are located at 0, 0, 0 (special position 16*c*) and aligned along the <111> direction at 295 K at 1.96(2) GPa. Neutron diffraction data suggest that at 120 K, upon pressure release down to 0.78(2) GPa, D_2 molecules start to rotate freely at 0, 0, 0. The recorded diffraction patterns indicate that there is no deuterium at site 8*a* ($\frac{1}{8}$, $\frac{1}{8}$, $\frac{1}{8}$). Measurements of the inclusion compound formation at 1.56(2) and 1.96(2) GPa permitted the determination of parameters in the Avrami model for the inclusion compound formation reaction. The Avrami exponent of 0.135(16) remains constant with pressure, indicating that the reaction's topochemistry is unaffected by pressure. The Avrami reaction rates of 0.29(3) and 0.23(3) min$^{-0.135}$ at 1.56(2) and 1.96(2) GPa, respectively, lead to a surprisingly low activation volume of the inclusion compound formation reaction of ~1.6 cm^3 mol^{-1}.

Experimental and methodological details

Experimental setup and neutron powder diffraction measurement description

Fine arsenolite powder (VEB Jenapharm – Laborchemie Apolda, used as received, see Fig. S1) was loaded into a gas clamp with D_2 at 2 kbar, applying a well-established offline high-pressure gas loading technique.[19] The sample was contained in a Cu single-toroidal gasket, which does not become embrittled in the presence of deuterium. The gasket volume was 13.7 mm^3, and 40–60% of its volume was occupied by arsenolite powder, which gives an $As_4O_6:D_2$ molar ratio ranging from 3.6 to 9.6. The gas clamp, equipped with zirconia-toughened alumina (ZTA) anvils, sealed the 2 kbar gas pressure before its use in a VX3 variant Paris-Edinburgh (PE) press.[20] Deuterium acted both as the reactant and the pressure-transmitting medium (PTM), and Pb powder was added to serve as a pressure marker.[21] The pressure estimated standard uncertainty was determined *via* error propagation, and its error is slightly underestimated because the error in the lead lattice parameter is underestimated by the Rietveld refinement.

We performed the time-of-flight (TOF) neutron powder diffraction measurements using a VX3 PE press on the PEARL instrument at the ISIS Neutron and Muon Source.[22] During the experiment, the PE press transmitted the hydraulic load *via* a pentane-driven piston, and the applied load on the press was progressively increased, ultimately generating a sample pressure of 1.5–2.0 GPa. Then, the clamp was left for a few hours, and diffraction data were collected to ensure complete transformation of arsenolite powder into its inclusion compound with deuterium. The sample temperature was subsequently lowered with the load on the press kept constant, and diffraction patterns were recorded at 250, 200, 150, and 120 K. The load on the press was then completely released, and the diffraction data were collected at 120 K. The PE press was then heated to room temperature. All diffraction data were collected in transverse mode.[22]

Data processing and profile refinements

Data processing involved initial attenuation correction using Mantid,[23] followed by Rietveld refinement with Topas V5.[24] A few refinements with a freely rotating D_2 molecule were carried out with Topas V7. The scattering factor of a freely rotating D_2 molecule, resulting in a spherically symmetric distribution of nuclear density around the molecular center,[25] is $F(Q) = 2b\sin(Qr_0)/Qr_0$, where F, Q, b and r_0 stand for the scattering factor, diffraction vector equal to $2\pi/d$, where d is the interplanar distance, deuterium neutron

diffraction length and D–D bond length (0.7415 Å).[11] The D atom was placed at 0, 0, 0 to get the correct position of the spherical distribution of nuclear density, and the correct scattering length b, while the remaining part of the scattering factor was applied using the `scale_occ` keyword in Topas V7. The 9.0–9.4 ms TOF section of the diffraction patterns (*ca.* 1.8–2.0 Å) contains a broad feature that comes from the CuBe impurity present in the Cu gasket. The CuBe phase was included as two components, corresponding to the same impurity scattering from two different locations of the gasket. These impurity reflections were also observed in the empty clamp (see Fig. S8 in ref. 26). Each phase, including the two CuBe components, was fitted using independent peak-shape functions. Preferred orientation was refined for CuBe and Al_2O_3 using spherical harmonics up to the 8th and 6th order, respectively. For alumina in the anvils, anisotropic peak asymmetry was also refined using spherical harmonics up to the 4th order. No preferred orientation nor anisotropic peak asymmetry was observed and refined for zirconia, also present in the anvils. In some patterns, a noticeable preferred orientation for arsenolite or its inclusion compound was observed and was refined with spherical harmonics up to the 8th order. All lattice parameters and atom positions unconstrained by symmetry were refined. Isotropic displacement parameters were not refined, except for arsenolite and/or its inclusion compound with deuterium, and were held constant at 0.5 $Å^2$, as their refinement yielded negative values. Simulations of the diffraction data were also carried out in Topas using the peak parameters derived from our experimental data. D atoms were placed manually in the structure to obtain the desired D_2 molecule orientations and a D–D bond length of 0.74 Å. No structure relaxation was performed. CIF files were produced using the Out_pdCIF macro.[27]

Kinetic investigation details

In Rietveld refinements for kinetic studies, atomic positions were not refined due to higher noise in the patterns collected for shorter times. Scales of arsenolite and its inclusion compound with deuterium were expressed as $S(1 - x)$ and Sx, respectively, where S is a common overall scale factor, and x is the conversion of arsenolite to the inclusion compound. The Avrami model was used to describe the conversion factor dependence on time: $x = 1 - e^{-b(t-t_0)^n}$ where $k = b^{1/n}$ is the reaction rate, n is a parameter related to the topochemistry of the reaction, and t_0 is the time between the reaction start and the beginning of diffraction measurements. Fitting of the Avrami equation parameters to experimental data was performed using Fit-o-mat software.[28]

Author contributions

Conceptualization: P. A. G.; funding acquisition: P. A. G.; investigation: P. A. G., M. D., C. L. B., C. J. R., and N. P. F.; methodology: P. A. G.; formal analysis: P. A. G. and C. J. R.; resources: P. A. G., C. L. B., C. J. R., and N. P. F.; writing – original draft: P. A. G., and writing – review & editing: all authors.

Conflicts of interest

There are no conflicts to declare.

Data availability

Raw neutron diffraction data are available at https://doi.org/10.5286/ISIS.E.RB2300013.

Supplementary information (SI): scanning electron micrograph of arsenolite powder, figure of Rietveld fit of the initial NPD pattern, additional figures of the kinetic data, cif files with the powder data. See DOI: https://doi.org/10.1039/d5ce01193k.

CCDC 2530234 and 2530235 contain the supplementary crystallographic data for this paper.[29a,b]

Acknowledgements

The research was supported by the Polish National Science Center, grant no. 2020/39/D/ST4/00128. Experiments at the ISIS Neutron and Muon Source were supported by a beamtime allocation RB2300013 from the Science and Technology Facilities Council. Invaluable help with the derivation of a structure factor of a freely rotating molecule, provided by Dr. Przemysław Górka, is gratefully acknowledged. A portion of this research was supported by resources at the Spallation Neutron Source, a DOE Office of Science User Facility operated by Oak Ridge National Laboratory (C. J. R.).

Notes and references

1 P. A. Guńka, K. F. Dziubek, A. Gładysiak, M. Dranka, J. Piechota, M. Hanfland, A. Katrusiak and J. Zachara, *Cryst. Growth Des.*, 2015, **15**, 3740–3745.
2 J. A. Sans, F. J. Manjón, C. Popescu, V. P. Cuenca-Gotor, O. Gomis, A. Muñoz, P. Rodríguez-Hernández, J. Contreras-García, J. Pellicer-Porres, A. L. J. Pereira, D. Santamaría-Pérez and A. Segura, *Phys. Rev. B*, 2016, **93**, 054102.
3 P. A. Guńka, M. Hapka, M. Hanfland, M. Dranka, G. Chałasiński and J. Zachara, *ChemPhysChem*, 2018, **19**, 857–864.
4 P. A. Guńka, M. Hapka, M. Hanfland, G. Chałasiński and J. Zachara, *J. Phys. Chem. C*, 2019, **123**, 16868–16872.
5 U.S. DRIVE Partnership, *Target Explanation Document: Onboard Hydrogen Storage for Light-Duty Fuel Cell Vehicles*, U. S. Department of Energy, Office of Energy Efficiency & Renewable Energy, Washington, DC, 2017.
6 P. A. Guńka, L. Zhu, T. A. Strobel and J. Zachara, *J. Chem. Phys.*, 2020, **153**, 054501.
7 P. A. Guńka, K. F. Dziubek and F. Capitani, *J. Phys. Chem. C*, 2023, **127**, 15871–15875.
8 M. Avrami, *J. Chem. Phys.*, 1939, **7**, 1103–1112.
9 M. Avrami, *J. Chem. Phys.*, 1940, **8**, 212–224.
10 M. Avrami, *J. Chem. Phys.*, 1941, **9**, 177–184.

11 K. P. Huber and G. M. Herzberg, in *NIST Chemistry WebBook*, ed. P. J. Linstrom and W. G. Mallard, National Institute of Standards and Technology, Gaithersburg MD, 2025.
12 S. F. Hulbert, *J. Br. Ceram. Soc.*, 1969, **6**, 11–20.
13 C. S. Yoo and M. Nicol, *J. Phys. Chem.*, 1986, **90**, 6732–6736.
14 A. Friedrich, I. E. Collings, K. F. Dziubek, S. Fanetti, K. Radacki, J. Ruiz-Fuertes, J. Pellicer-Porres, M. Hanfland, D. Sieh, R. Bini, S. J. Clark and T. B. Marder, *J. Am. Chem. Soc.*, 2020, **142**, 18907–18923.
15 K. Shirzad and C. Viney, *J. R. Soc., Interface*, 2023, **20**, 20230242.
16 P. Yi, M. L. Falk and T. P. Weihs, *J. Appl. Phys.*, 2018, **124**, 165303.
17 S. Sadi, A. Hanna, T. Baudin, A.-L. Helbert, F. Brisset, D. Bradai and H. Azzeddine, *J. Met., Mater. Miner.*, 2022, **32**, 12–26.
18 F. Safari, M. Tkacz and A. Katrusiak, *J. Phys. Chem. C*, 2021, **125**, 7756–7762.
19 S. Klotz, J. Philippe, C. L. Bull, J. S. Loveday and R. J. Nelmes, *High Pressure Res.*, 2013, **33**, 214–220.
20 S. Klotz, G. Hamel and J. Frelat, *High Pressure Res.*, 2004, **24**, 219–223.
21 A. D. Fortes, *A revised equation of state for in situ pressure determination using fcc-Pb (0 < P < 13 GPa, T> 100 K)*, STFC, 2019.
22 C. L. Bull, N. P. Funnell, M. G. Tucker, S. Hull, D. J. Francis and W. G. Marshall, *High Pressure Res.*, 2016, **36**, 493–511.
23 O. Arnold, J. C. Bilheux, J. M. Borreguero, A. Buts, S. I. Campbell, L. Chapon, M. Doucet, N. Draper, R. Ferraz Leal, M. A. Gigg, V. E. Lynch, A. Markvardsen, D. J. Mikkelson, R. L. Mikkelson, R. Miller, K. Palmen, P. Parker, G. Passos, T. G. Perring, P. F. Peterson, S. Ren, M. A. Reuter, A. T. Savici, J. W. Taylor, R. J. Taylor, R. Tolchenov, W. Zhou and J. Zikovsky, *Nucl. Instrum. Methods Phys. Res., Sect. A*, 2014, **764**, 156–166.
24 A. A. Coelho, *J. Appl. Crystallogr.*, 2018, **51**, 210–218.
25 K. A. Lokshin, Y. Zhao, D. He, W. L. Mao, H.-K. Mao, R. J. Hemley, M. V. Lobanov and M. Greenblatt, *Phys. Rev. Lett.*, 2004, **93**, 125503.
26 Z. Wei, N. P. Funnell, C. J. Ridley, S. Klotz, C. R. Pulham and C. L. Bull, *Inorg. Chem.*, 2026, **65**, 631–637.
27 M. R. Rowles, *J. Appl. Crystallogr.*, 2022, **55**, 631–637.
28 A. Möglich, *J. Chem. Educ.*, 2018, **95**, 2273–2278.
29 (*a*) CCDC 2530234: Experimental Crystal Structure Determination, 2026, DOI: 10.5517/ccdc.csd.cc2qxxg1; (*b*) CCDC 2530235: Experimental Crystal Structure Determination, 2026, DOI: 10.5517/ccdc.csd.cc2qxxh2.